THE ASTROPHYSICAL JOURNAL, 582:L35–L38, 2003 January 1

MID-INFRARED IMAGING POLARIMETRY OF NGC 7027

C. A. JURGENSON,[1] R. E. STENCEL,[1] D. S. THEIL,[1] D. I. KLEBE,[1] AND T. UETA[2,3]
Received 2002 August 19; accepted 2002 November 19; published 2002 November 27

ABSTRACT

We present mid-infrared imaging polarization vector diagrams of the young planetary nebula NGC 7027. The observations were taken with the University of Denver's Ten and Twenty μm Camera at the Wyoming Infrared Observatory. Individual wave plate position images have been deconvolved to remove the instrument point-spread function. The deconvolved 9–13 μm intensity images, in 1 μm wide bandpasses, show a bright ellipsoidal double-peaked core surrounded by a region of fainter emission, consistent with recent continuum images in the near-infrared. The vector diagrams show significant changes in polarization position angle with wavelength, suggesting scattering from large grains.

Subject headings: circumstellar matter — infrared: ISM — instrumentation: polarimeters — planetary nebulae: individual (NGC 7027) — polarization

1. INTRODUCTION

The role of mass loss from low to intermediate (0.8–8 $M_{\odot}$) initial mass stars is a topic of considerable interest in stellar evolution because of its effect upon the structure/composition of the circumstellar envelope and subsequent evolution into a planetary nebula (PN). Much work has been done to better our understanding through spectroscopy and imaging across the spectrum, but little has been done in the mid-infrared (mid-IR) using polarimetry as a technique in studying mass loss. Most of the polarimetric work in the mid-IR has been done on the Galactic center, Orion-BN, and young stellar objects (Dyck et al. 1973; Dyck & Beichman 1974; Aitken et al. 1985, 1986; Smith et al. 2000) and into understanding the grain alignment mechanisms (Davis & Greenstein 1951; Gold 1952; Purcell & Spitzer 1971; Harwit 1971). Martin (1975), using polarization observations of the BN source in Orion, was able to place constraints on the shape, degree of alignment, and composition of the dust grains in the interstellar matter (ISM). Li & Mayo Greenberg (2002) predict that mid-IR spectropolarimetry can constrain the core-mantle interstellar dust model.

Johnson & Jones (1991) studied near-IR polarization characteristics from a sample of red giants to planetary nebulae (PNs). They found that polarization increases with age from the asymptotic giant branch (AGB) to the post-AGB phase and then decreases with increasing PN age. They also noted that aspherical mass loss is a continual feature in the late stages of stellar evolution and that the axisymmetric morphology we often observe in PNs most likely begins as early as the AGB (cf. Stencel 2000). Symmetry breaking of circumstellar shells near the end of the AGB phase has most recently been confirmed by Ueta, Meixner, & Bobrowsky (2000). Thermal emission from evolved stars is dominated by dust continuum from warm dust grains, which can also scatter radiation into preferred directions depending on their alignment with respect to the central star. Polarization studies of the late stages of AGB stars and the early stages of PNs can then help to reveal grain properties and the alignment mechanisms behind the changes in mass loss and envelope geometry responsible for their shaping.

NGC 7027 presents the unique case of a nearby young PN (880 $\pm$ 150 pc, dynamical age 600 yr; Masson 1989) that has been extensively studied across the spectrum. The PN's complex morphology consists of an elliptical ionized core that is surrounded by an extended molecular envelope (Bieging, Wilner, & Thronson 1991). Latter et al. (2000), using *Hubble Space Telescope* (*HST*) Near-Infrared Camera and Multi-Object Spectrometer (NICMOS) images, derived a central stellar temperature of 198,000 K and suggested the presence of a major disruption at P.A. $\sim 53°$ (with position angles as defined by Cox et al. 2002), running northwest-southeast corresponding to a fast collimated outflow or jetlike structure. This jet is also present in *HST* images (Ciardullo et al. 1999) and in the X-ray (Kastner, Vrtilek, & Soker 2001). In this Letter, we present the first mid-IR imaging polarimetry of NGC 7027.

2. OBSERVATIONS AND DATA REDUCTION

NGC 7027 was observed using the Ten and Twenty μm Camera (TNTCAM2) at the Wyoming Infrared Observatory (WIRO) on 2001 June 6 in four 1 μm wide bandpasses centered on 9.7, 10.6, 11.7, and 12.6 μm. The WIRO f/28, 2.3 m telescope provides 0.″78 pixel^{-1} at the detector and pointing stability of 0.″1 pixel^{-1} rms in declination and 0.″2 pixel^{-1} rms in right ascension. The detector used is a He-cooled Boeing 128 × 128 arsenic-doped silicon (Si:As) blocked impurity band (BIB) array with high sensitivity at wavelengths between 5 and 25 μm. A unique feature of TNTCAM2 is that all mechanical motion, polarization optics, and filters are within the cryostat at 8 K. For a thorough description of the instrument and its operation, see Klebe, Stencel, & Theil (1998).

For each bandpass, the linear polarization was calculated from four chop/nod subtracted intensity images, one for each half-wave plate rotation position over a stationary wire grid. The telescope secondary was chopped at 10 Hz for rapid sky fluctuation subtraction and nodded for the purpose of beam switching to subtract out any residuals in the background due to telescope, instrument, and surrounding environment. The chop/nod throws were such that the image was kept on the array so that after the subtraction was performed, there were four images for a given wave plate position to be spatially registered and co-added. Since there were no IR bright point sources available for automated centroiding, registration was performed by expanding the images by 20 times and examining in detail features within the nebula. Structural features above

[1] Department of Physics and Astronomy, University of Denver, 2112 East Wesley Avenue, Denver, CO 80208; cjurgens@du.edu.
[2] Department of Astronomy, University of Illinois at Urbana-Champaign, 1002 West Green Street, Urbana, IL 61801.
[3] Current address: Royal Observatory of Belgium, Ringlaan 3, 1180 Brussels, Belgium; ueta@oma.be.

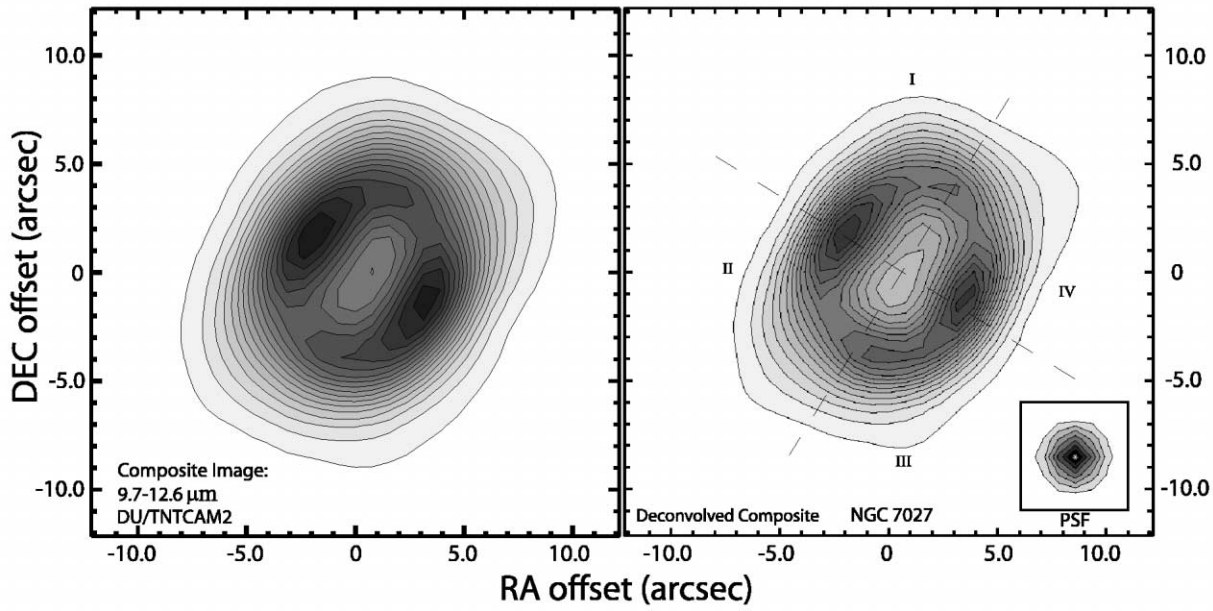

FIG. 1.—*Left*: Composite 9–13 μm image. *Right*: Deconvolved composite image; *inset*: instrument PSF used for deconvolution. The brightest contours of the double-peaked elliptical core have a S/N of 226 with respect to the pixel-to-pixel noise level of ± 1340 counts; the center region yields S/N of 78 and the last exterior contour 50. For the PSF, the pixel-to-pixel noise level is $\pm 12{,}539$ counts; the central contour has a S/N of 3750 and the last contour 32.

a given count of detector units were used to create subarrays centered on a given pixel whose position was geometrically determined to be consistent within the nebula in all wave plate position images and bandpasses. This provided pixel-to-pixel correspondence, not only for the four individual chop/nod images but amongst the wave plate position images as well. Polarization caused by image drift, pointing stability, or image shift due to wave plate rotation is then minimized.

In a given filter, the sequence of observations in terms of wave plate positions was $Q1$-$Q2$-$Q2$-$Q1$-$U1$-$U2$-$U2$-$U1$, where $Q1$ and $Q2$ are intensity images with wave plate fast axis at 0° and 45° with respect to the wire grid, and $U1$ and $U2$ are intensity images with the fast axis at 22.5 and 67.5 with respect to the wire grid. $Q1$, $Q2$, $U1$, and $U2$ provide independent measures of the total intensity, so the analysis was done in terms of the reduced Stokes parameters defined by $q = (Q1 - Q2) / (Q1 + Q2)$ and $u = (U1 - U2) / (U1 + U2)$. Each wave plate position image is composed of four images that are background sky and instrument subtracted. Each chop pair (from the two nod positions) consists of 128 frames at 0.04 s integration time for bandpasses centered on 10.6 and 12.6 μm and 0.05 s integration time for bandpasses centered on 9.7 and 11.7 μm. The four chop/nod images were then coadded, yielding wave plate images with total integration times of 10.2 s for the 10.6 and 12.6 μm bandpasses and 12.8 s for the 9.7 and 11.7 μm bandpasses.

IR bright photometric standard stars were also observed in the polarimetry mode of TNTCAM2 to measure the instrumental polarization. Values of polarization magnitude between 1% and 1.5% were measured. Among the five photometric standard stars that were observed over the four night observing run in which NGC 7027 also was observed, HD 206936 (see inset of Fig. 1, *right*) was observed concurrently with NGC 7027. This was also the star used to provide the instrument point-spread function (PSF) in the deconvolution routine, following the method described by Kastner et al. (2002). The photometric standard stars also were imaged on different parts of the array, resulting in no noticeable difference in instrumental polarization with position. Polarimetry vector diagrams were produced in all but the 9.7 μm bandpass because of the necessity of high signal-to-noise ratio (S/N) required for confidence in polarimetric measurements.

As stated above, the instrument PSF was deconvolved out of the individual wave plate position images in every filter before the calculation of Stokes parameters. The maximum likelihood method was applied using a routine from the IDL Astronomy Library, and convergence was found after seven iterations.

Figure 1 (*left and right*) shows the undeconvolved and deconvolved composite intensity maps summed over all bandpasses of NGC 7027. Noticeable features include the two-peaked bright ellipsoidal core, P.A. oriented ~32° west of north, which is consistent with recent spectral imaging by Cox et al. (2002), plus fainter emission that extends within and beyond the elliptical core. Also noticeable is a disruption in the brightness distribution that runs northwest-southeast corresponding to the outflow structure as mentioned by Latter et al. (2000). The long axis of the fainter emission extending outside the elliptical core is offset from the elliptical core major axis by 4° at P.A. ~ 28° west of north and roughly aligns with the axis of the quadropolar H_2 emission seen in the near-IR (Latter et al. 2000; Cox et al. 2002). The image has features similar to continuum images at 2 and 3.28 μm (Cox et al. 2002 and Graham et al. 1993, respectively).

Figure 2 displays the undeconvolved vector diagrams (*top, left to right*) and the deconvolved diagrams (*bottom, left to right*), with vectors plotted for each pixel with a S/N $\geq$ 60. Most pixels show polarization in excess of measured instrumental values. We checked contamination due to mid-IR lines in each band using spectral information obtained by the *Infrared Space Observatory* (*ISO*) short-wavelength spectrometer (SWS; Bernard-Salas et al. 2001; Hony et al. 2001): 10.6 μm is continuum dominated with the addition of a weak [S IV] line at 10.5 μm whose emission is less than 5% of the continuum; 11.7 μm is continuum plus polycyclic aromatic hydrocarbon (PAH) emission at 11.2 μm with a relative strength of about

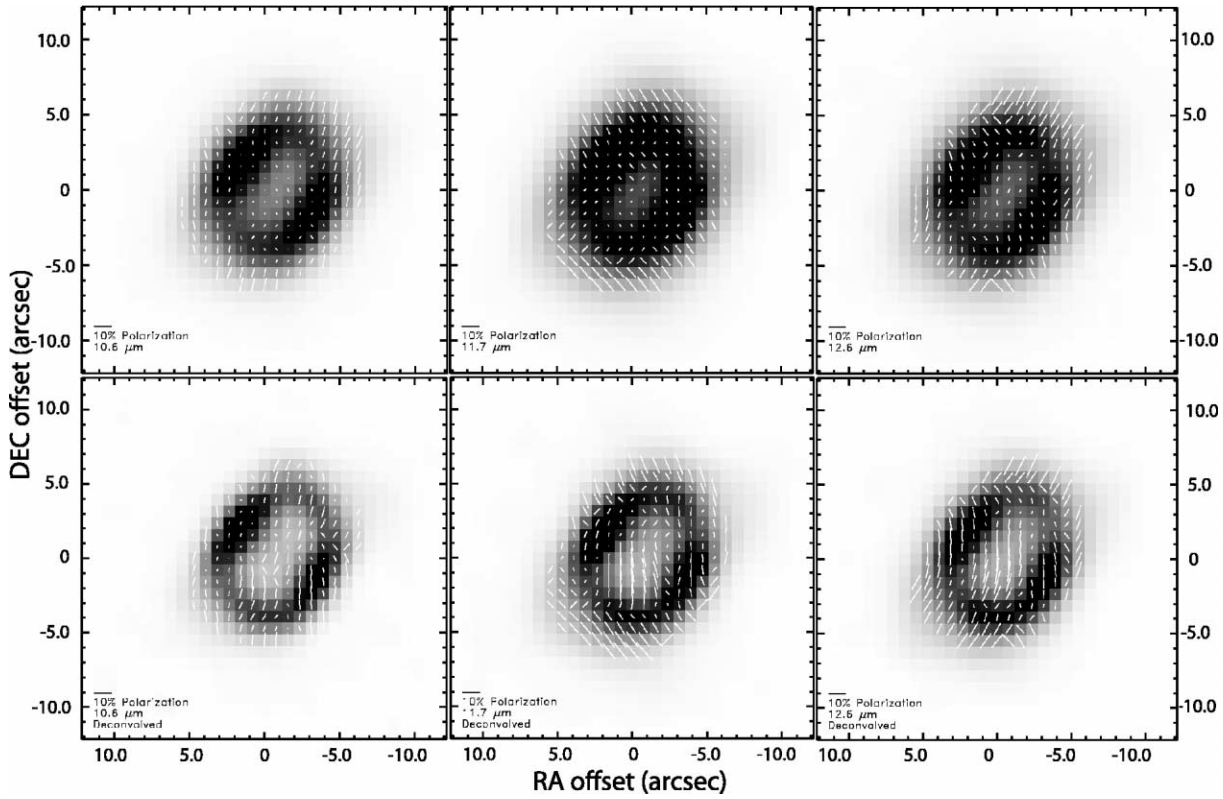

FIG. 2.—*Top*: Undeconvolved polarization vector diagrams. *Bottom*: Deconvolved diagrams.

25%; 12.6 μm is again continuum dominated but has a PAH feature at 12.8 μm with a relative strength of about 5%.

3. DISCUSSION

The polarization vector diagrams (Fig. 2) show important differences depending on relative strength of line and continuum and azimuthal position relative to the outflow structure as described by Latter et al. (2000). If we divide each diagram into four quadrants, I–IV (see Fig. 1, *right*), by the lines of the semimajor/semiminor axis of the ellipse, we can more readily compare the polarization magnitudes and position angles among the diagrams. One immediate observation is that that magnitude of polarization is larger in the bands that contain the PAH features. In the south quadrant (III) of the 10.6 and 12.6 μm images, the diagrams exhibit polarization vectors that are more or less radial, while the 11.7 μm diagram, with the strongest PAH contribution, has polarization vectors that are roughly tangential. Hence, significant polarization differences with position and wavelength have been found. The only significant difference between the two sets of diagrams is that in the deconvolved diagrams, the bright center of the nebula, with S/N above 80, shows detection of polarization vectors that better define the core after deconvolution.

In the mid-IR, wavelengths of radiation are generally much longer than the physical scale of the grains, if we assume 0.1 μm sized grains as in models of NGC 7027 (e.g., Volk & Kwok 1997). Then, scattering can be assumed to be negligible, since its efficiency decreases with increasing wavelength and thermal emission is considered to be the dominant polarizing process by the grains. However, this would not hold if much larger grains exist and scattering can no longer be negligible. The presence of large grains (a few hundred μm and up to 1 cm) has been suggested in the circumstellar shells of post-AGB stars through observations (e.g., Jura et al. 2000) and radiative transfer calculations (e.g., Meixner et al. 2002). In the dust nebula of this young PN, NGC 7027, there still may be many large grains that are being refined into smaller pieces, such as the ones found in the ISM. If this is the case, scattering by grains can also be a source of polarization at the mid-IR wavelengths.

Polarization due to scattering could explain the observed change in position angles of the polarization among the three bandpasses, since polarization position angles are independent of wavelength only if the measurements that sample the same column of dust are free of contributions from scattering (Hildebrand 1988). Hony et al. (2001) compared the laboratory spectrum with observations of PAH features in NGC 7027 and hypothesized that the 11.2 μm feature is due to large molecules with 100–200 C atoms and long straight edges. Smith et al. (2000), commenting on unpublished data from the Orion bar and NGC 7027, have placed upper limits (1%) on the polarization contributions from the 11.2 μm PAH emission. The measurements of Smith et al. (2000) would seem to rule out the possibility of the observed change in the position angles being due solely to PAH emission, although Holloway et al. (2002) detect significant polarization from a 3.47 μm carbonaceous feature in the BN object. Hence, the observed polarization at mid-IR wavelengths in NGC 7027 seems to arise from two competing polarization processes, thermal emission and scattering by dust grains, suggesting the presence of large dust grains. Clearly, further study is needed.

4. SUMMARY

We have presented mid-IR imaging polarimetry results on the young PN, NGC 7027. The two-peaked core structure surrounded by a faint extended nebulosity in the mid-IR intensity

map is consistent with previous optical and near-IR observations. Comparing the three polarization vector diagrams and the suggested differential polarization contribution from PAH species in the 11.7 μm image, we suggest that the difference in the polarization position angles with wavelength in these images is due to the presence of large grains in the nebula of NGC 7027. This is reasonable, given that NGC 7027 is a very young PN and large grains may still be present in its nebula, as is the case in post-AGB shells.

These are initial results of the polarimetry mode of TNTCAM2 and, as far as we know, the first imaging polarization observations of this famous nebula. The initial goal of the investigation was to see if we could detect polarized signal from evolved extended sources. That being done, it should then be possible to infer the alignment mechanism as well as put constraints on grain shape, degree of alignment, and composition.

We would like to acknowledge Craig H. Smith for helpful conversations about polarimetry and the referee for valuable suggestions. We also thank the University of Wyoming Department of Physics and Astronomy for access to WIRO, especially Paul Johnson, Jim Weger, Rich Coley, and Ray Martin for support of the observing run with TNTCAM2. We also acknowledge NSF grant AST 97-24506 to the University of Denver for TNTCAM2 construction and the estate of William Herschel Womble.

REFERENCES

Aitken, D. K., Bailey, J. A., Roche, P. F., & Hough, J. M. 1985, MNRAS, 215, 815
Aitken, D. K., Roche, P. F., Bailey, J. A., Briggs, G. P., Hough, J. H., & Thomas, J. A. 1986, MNRAS, 218, 363
Bernard-Salas, J., Pottasch, S. R., Beintema, D. A., & Wesselius, P. R. 2001, A&A, 367, 949
Bieging, J. H., Wilner, D., & Thronson, H. A. 1991, ApJ, 379, 271
Ciardullo, R., Bond, H. E., Sipior, M. S., Fullton, L. K., Zhang, C. Y., & Schaefer, K. G. 1999, AJ, 118, 488
Cox, P., Huggins, J. P., Maillard, J.-P., Habart, E., Morisset, C., Bachiller, R., & Forveille, T. 2002, A&A, 384, 603
Davis, L., & Greenstein, J. L. 1951, ApJ, 114, 206
Dyck, H. M., & Beichman, C. A. 1974, ApJ, 194, 57
Dyck, H. M., Capps, R. W., Forrest, W. J., & Gillett, F. C. 1973, ApJ, 183, L99
Gold, T. 1952, MNRAS, 112, 215
Graham, J. R., Serabyn, E., Herbst, T. M., Matthews, K., Neugebauer, G., Soifer, B. T., Wilson, T. D., & Beckwith, S. 1993, AJ, 105, 250
Harwit, M. 1970, Bull. Astron. Inst. Czechoslovakia, 21, 204
Hildebrand, R. H. 1988, QJRAS, 29, 327
Holloway, R. P., Chrysostomou, A., Aitken, D. K., Hough, J. H., & McCall, A. 2002, MNRAS, 336, 425
Hony, S., Van Kerckhoven, C., Peeters, E., Tielens, A. G. G. M., Hudgins, D. M., & Allamandola, L. J. 2001, A&A, 370, 1030
Johnson, J. J., & Jones, T. J. 1991, AJ, 101, 1735
Jura, M., Turner, J. L., Van Dyk, S., & Knapp, G. R. 2000, ApJ, 528, L105
Kastner, J. H., Li, J., Siebenmorgen, R., & Weintraub, D. A. 2002, AJ, 123, 2658
Kastner, J. H., Vrtilek, S. D., & Soker, N. 2001, ApJ, 550, L189
Klebe, D. I., Stencel, R. E., & Theil, D. S. 1998, Proc. SPIE, 3354, 853
Latter, W. B., Dayal, A., Bieging, J. H., Meakin, C., Hora, J. L., Kelly, D. M., & Tielens, A. G. G. M. 2000, ApJ, 539, 783
Li, A., & Mayo Greenberg, J. 2002, ApJ, 577, 789
Martin, P. G. 1975, ApJ, 202, 393
Masson, C. R. 1989, ApJ, 336, 294
Meixner, M., Ueta, T., Bobrowsky, M., & Speck, A. 2002, ApJ, 571, 936
Purcell, E. M., & Spitzer, L. 1971, ApJ, 167, 31
Smith, C. H., Wright, C. M., Aitken, D. K., Roche, P. F., & Hough, J. H. 2000, MNRAS, 312, 327
Stencel, R. E. 2000, in ASP Conf. Ser. 199, Asymmetric Planetary Nebulae II, ed. J. H. Kastner, N. Soker, & S. Rappaport (San Francisco: ASP), 99
Ueta, T., Meixner, M., & Bobrowsky, M. 2000, ApJ, 528, 861
Volk, K., & Kwok, S. 1997, ApJ, 477, 722